

MISMO FIELD EXPERIMENT IN THE EQUATORIAL INDIAN OCEAN*

BY KUNIO YONEYAMA, YUKIO MASUMOTO, YOSHIFUMI KURODA, MASAKI KATSUMATA, KEISUKE MIZUNO, YUKARI N. TAKAYABU, MASANORI YOSHIZAKI, ALI SHAREEF, YASUSHI FUJIYOSHI, MICHAEL J. MCPHADEN, V. S. N. MURTY, RYUICHI SHIROOKA, KAZUAKI YASUNAGA, HIROYUKI YAMADA, NAOKI SATO, TOMOKI USHIYAMA, QOOSAKU MOTEKI, AYAKO SEIKI, MIKIKO FUJITA, KENTARO ANDO, HIDEAKI HASE, IWAO UEKI, TAKANORI HORII, CHIE YOKOYAMA, AND TOMOKI MIYAKAWA

In situ atmospheric and oceanic measurements reveal the complexity of physical processes during initiation of convection associated with intraseasonal variability in the central equatorial Indian Ocean.

This article describes the Mirai Indian Ocean cruise for the Study of the Madden-Julian oscillation (MJO)-convection Onset (MISMO) observational campaign, the goal of which was to study the onset mechanism of convection in the MJO (Madden and Julian 1971, 1972) in the equatorial Indian Ocean. The MJO is the dominant intraseasonal (i.e., periods of 30–60 days) variation in the tropics. It is characterized by eastward-propagating disturbances in the atmosphere, with deep atmospheric convection primarily evident over the warm pool region from the central Indian Ocean to the western Pacific Ocean in the boreal winter–spring season (see sidebar for a schematic diagram of the MJO convection). In addition to its important role in regulating the tropical climate, the MJO has a strong impact on higher latitudes through interaction with monsoons (e.g., Yasunari 1979; Hendon and Liebmann 1990), El Niño (e.g., Nitta and Motoki 1987; McPhaden 1999), tropical cyclones (e.g., Liebmann et al. 1994; Maloney and Hartmann 2001), and others. The MJO also has substantial impact on ►

A Maldives Atoll in the central Indian Ocean.

*National Institute of Oceanography
Contribution Number 4378.

weather along the west coast of the United States (Bond and Vecchi 2003). Furthermore, because of its prominence, the MJO is often used as a test bed to evaluate the performance of the general circulation models (GCMs; Slingo et al. 1996; Lin et al. 2006). Therefore, accurate knowledge of the MJO is important not only for understanding the current climate but also for improving weather and climate prediction.

Explaining the initiation process of MJO convection has been a major concern of MJO studies since its discovery. Although many hypotheses have been proposed (e.g., Hsu et al. 1990; Wang and Li 1994; Hu and Randall 1994; Raymond 2001; Kemball-Cook and Weare 2001; Sperber 2003), there has been no universally agreed upon definitive explanation. Most of these hypotheses were derived from numerical model or analytical studies using global-scale datasets such as satellite and reanalysis data. Recently, Tian et al. (2006) found significant discrepancies in moisture and temperature structure in the lower troposphere between satellite and NCEP–NCAR reanalysis^{*1} over the oceans, because of insufficient in situ observation data to constrain the reanalysis. Although in situ data taken during the field experiment TOGA COARE^{*} have been used for the study of MJO convection (e.g., Lin and Johnson 1996), they did not elucidate onset mechanisms, because the field work was conducted in the tropical western Pacific Ocean while most MJO convection is initiated over the Indian Ocean.

In addition, oceanic processes are also important in the study of MJO variability as air–sea interaction is thought to be a key component of the evolution of the MJO convection (e.g., Krishnamurti et al. 1988; Woolnough et al. 2007). The MJO also greatly influences ocean surface structures such as sea surface

temperature (SST) and zonal current (e.g., Han et al. 2001; Waliser et al. 2003). Masumoto et al. (2005) demonstrated using mooring current data at 0°, 90°E that intraseasonal disturbances dominated in the zonal current in the eastern equatorial Indian Ocean. They pointed out that this intraseasonal variability of zonal current was associated with the MJO and might strongly modulate the eastward upper-ocean currents along the equator known as the Wyrtki jet^{*} (Wyrtki 1973), which appear twice a year during the monsoon transition periods (April–May and October–November). In addition, intraseasonal disturbances in the zonal current may influence Indian Ocean Dipole (IOD) events^{*} (Saji et al. 1999), but the relationship between them still remains unresolved.

As mentioned above, the exact mechanisms governing the MJO are the subject of active debate and research, so comprehensive observational datasets in the Indian Ocean are needed to address the many possibilities. To meet these scientific needs, the Japan Agency for Marine–Earth Science and Technology (JAMSTEC) conducted a field experiment in October–December 2006, focusing on the initiation of convection in the MJO in the central equatorial Indian Ocean, and named this project MISMO. This article will describe the details of the observations as well as several early results with focus on atmospheric features. A brief implementation plan can be found in Yoneyama et al. (2006).

EXPERIMENT OBJECTS. The aim of MISMO was to describe and understand atmospheric and oceanic conditions in the central equatorial Indian Ocean when convection in the MJO was initiated. To conduct the observations effectively with the limited resources, we concentrated MISMO on a subset of issues. Previous studies have suggested what kinds of measurements are key to understanding the

¹ Terms marked with asterisks are defined in the appendix.

AFFILIATIONS: YONEYAMA, KATSUMATA, MIZUNO, YOSHIZAKI, SHIROOKA, YASUNAGA, YAMADA, SATO, USHIYAMA, MOTOKI, SEIKI, FUJITA, ANDO, HASE, UEKI, AND HORII—IORGC, JAMSTEC, Yokosuka, Japan; MASUMOTO—IORGC, JAMSTEC, Yokosuka, and Department of Earth and Planetary Sciences, University of Tokyo, Tokyo, Japan; KURODA[#]—Marine Technology Center, JAMSTEC, Yokosuka, Japan; TAKAYABU—Center for Climate System Research, University of Tokyo, Kashiwa, and IORGC, JAMSTEC, Yokosuka, Japan; SHAREEF—National Meteorological Center, Male, Maldives; FUJIYOSHI—Hokkaido University, Sapporo, Japan; MCPHADEN—Pacific Marine Environmental Laboratory, National Oceanic and Atmospheric Administration, Seattle, Washington; MURTY—National Institute of Oceanography, Goa, India; YOKOYAMA AND MIYAKAWA—Center for Climate System Research, University of Tokyo, Kashiwa, Japan

***#CURRENT AFFILIATIONS:** USHIYAMA—National Institute for Agro–Environmental Sciences, Tsukuba, Japan; KURODA—Nippon Marine Enterprises Ltd., Yokosuka, Japan

CORRESPONDING AUTHOR: Kunio Yoneyama, Institute of Observational Research for Global Change (IORGC)/Japan Agency for Marine–Earth Science and Technology (JAMSTEC), 2-15, Natsushima-cho, Yokosuka 237-0061, Japan
E-mail: yoneyamak@jamstec.go.jp

The abstract for this article can be found in this issue, following the table of contents.

DOI:10.1175/2008BAMS2519.1

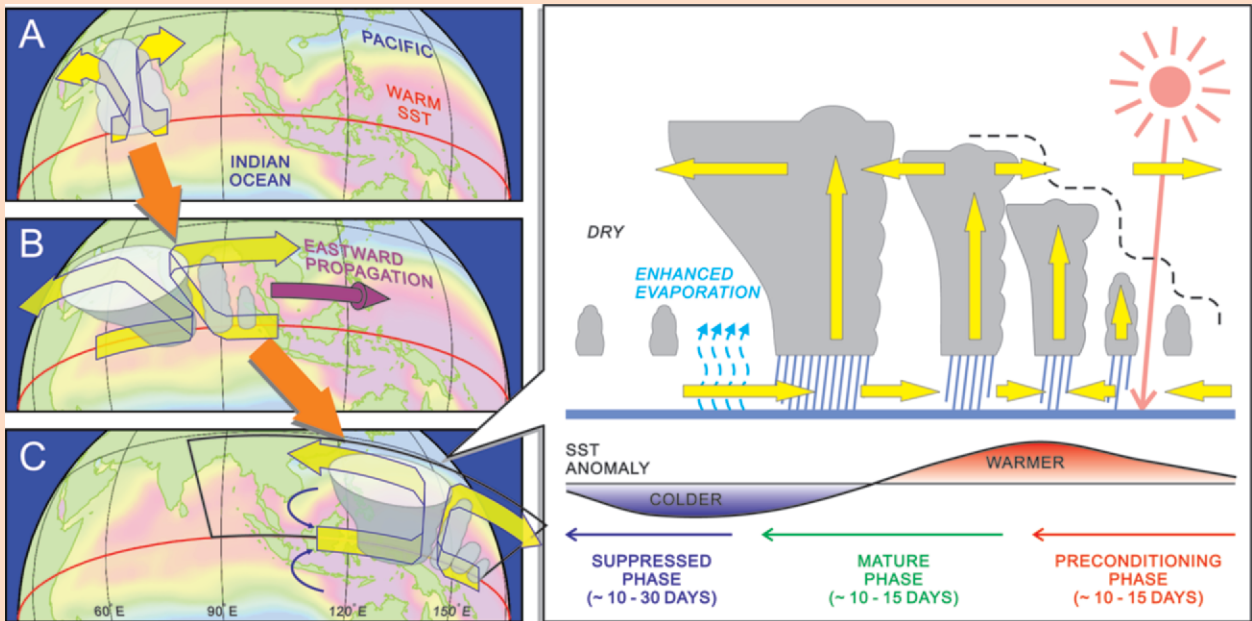
In final form 1 May 2008
©2008 American Meteorological Society

initiation of convection in the MJO. For example, Johnson et al. (1999) showed the existence of the trimodal cloud distribution with shallow cumulus, congestus, and deep cumulonimbus over the tropical western Pacific Ocean. In particular, it was shown that congestus clouds that developed during the convectively suppressed period of the MJO played a key role for the moistening of the midtroposphere and preconditioned it for the active phase of the MJO with deep convection (Johnson et al. 1999; Kikuchi and Takayabu 2004). In addition, the diurnal cycle

of the sea surface temperature in light wind conditions seems to be crucial for the initiation of shallow cumulus and congestus clouds. These results suggest that the coupling between the atmosphere and the upper ocean plays an important role for the initiation of MJO convection (Slingo et al. 2003; Bernie et al. 2005). In addition to these local vertical features, low-level moisture convergence is also a key component in studying the development of tropical convection (e.g., Maloney and Hartmann 1998; Seo and Kim 2003).

SCHEMATIC DIAGRAM OF THE MJO CONVECTION

Yellow arrows indicate the circulation in the zonal plane along the equator. (left) Typical development (A to B) and movement (B to C) of the MJO convection in the spatial coordinates. (right) Time evolution of convection based on the recharge–discharge theory (Bladé and Hartmann 1993) and other relevant observational studies (e.g., Lin and Johnson 1996; Kemball-Cook and Weare 2001). Time axis is from right to left and full length indicates the intraseasonal time scale with three different convective phases of preconditioning (red), mature (green), and suppressed (blue) as shown by arrows at the bottom. Curve with red/blue shading indicates the positive/negative SST anomaly from the intraseasonal mean (horizontal line).



These figures contain some of the basic observed features of the MJO based on the review paper by Zhang (2005), which include the following:

- 1) intraseasonal variability at 30–60-day periods;
- 2) eastward propagation along the equator with a phase speed of $\sim 5 \text{ m s}^{-1}$ in the Eastern Hemisphere;
- 3) zonal wave number 1–6;
- 4) frequent initiation of convection in the Indian Ocean and termination over relatively cold surface water in the central Pacific Ocean;
- 5) weakening of convective activity over the maritime continent region;
- 6) baroclinic zonal wind structure with westerly/easterly in the lower/upper troposphere to the west of convective center;
- 7) westward tilt with height of many variables such as water vapor, divergence, diabatic heating, and so on;
- 8) multiscale structure with mesoscale [$O(10^2 \text{ km})$] convective systems within a large-scale [$O(10^3 \text{ km})$] cloud envelope; and
- 9) frequent appearance of Rossby gyre (equatorward flow from both hemispheres) in the lower troposphere to the west of convective center (blue arrows in C).

By considering these studies as well as others mentioned in the introduction, we focused on the following themes as the experiment objectives:

- the time evolution of moisture convergence in the lower troposphere and vertical profiles of atmospheric parameters such as water vapor, wind, and clouds;
- air–sea interaction with focus on the diurnal cycle of sea surface temperature; and
- variations of ocean surface structures including surface currents and the mixed layer heat budget.

PLATFORMS AND MEASUREMENT SYSTEMS. To capture atmospheric and oceanic characteristics of the central equatorial Indian Ocean from the viewpoint of our experiment objectives, the observation network was constructed with the research vessel (R/V) *Mirai*, land-based sites at the Maldives Islands, and moored buoys. Details are summarized below.

R/V Mirai. The major component of this campaign was to send the *R/V Mirai* to the Indian Ocean to conduct the observations in the open ocean. The *Mirai* is one of the largest research vessels, whose length is about 130 m and gross tonnage is 8,687 ton (Fig. 1). Because of this huge capacity and active antirolling system, it is very stable and various measurements can be conducted on its wide deck. In addition, although the *R/V Mirai* belongs to JAMSTEC, she is operated as a mission-oriented ship, and non-JAMSTEC researchers can also join cruises through a prescribed public selection process. This operation style makes it possible to conduct a variety of observations. Table 1 summarizes the observations conducted on board the *Mirai*. In addition to these in situ measurements, a numerical modeling group (principal investigator: T. Shinoda, Nagoya University) also joined the campaign.

The main mission of the *R/V Mirai* was to conduct intensive observations using Doppler radar, radio-sondes, a conductivity–temperature–depth (CTD) system, and other measurements around a fixed

site (0°, 80.5°E) for about 1 month. The *R/V Mirai* cruise track and the intensive observation network are depicted in Fig. 2. Before arriving at the main site, 12 Argo floats were deployed along the 80°E section from 8°S to 3°N. Argo floats usually measure temperature and salinity from 1,500 m or deeper to the surface every 10 days. However, 10 of these floats were programmed to observe temperature and salinity above 500 m every day with 2-m vertical resolution to capture the intraseasonal variability of the upper ocean in detail.

The *R/V Mirai* stayed within a buoy array area from 24 October to 25 November (33 days), and most observations were conducted at 0°, 80.5°E from 28 October through 21 November 2006 (25 days). Hereafter, we refer to the 33-day period as the “stationary observation period.” In addition, we define



FIG. 1. R/V Mirai. Numbers indicate the locations of instruments listed in Table 1.

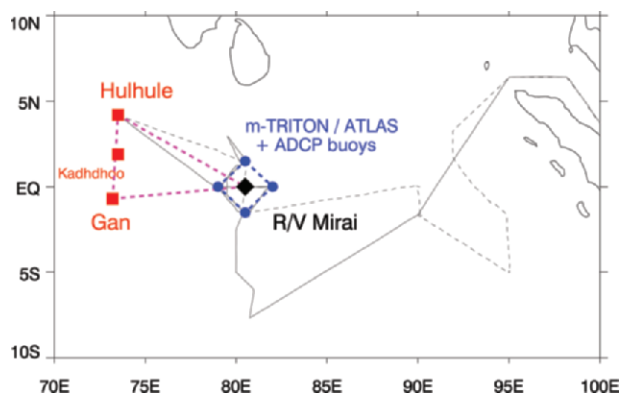


FIG. 2. Observation network with atmospheric sounding array (red, dashed) and oceanic buoy array (blue, dashed). Black thin solid and dashed lines indicate the cruise tracks of the R/V Mirai for leg 1 and leg 2. Solid diamond indicates the stationary observation site at 0°, 80.5°E.

the intensive observation period (IOP) as the time when the R/V *Mirai* cruised the Indian Ocean from 19 October through 10 December (53 days).

Moored buoy array. To capture the upper-ocean variability, a moored buoy array was deployed. Positions, observation periods, and other information are briefly summarized in Table 2. Surface meteorological and oceanographic parameters were monitored by two mini-Triangle Trans-Ocean Buoy Network (m-TRITON) buoys and three Autonomous Temperature Line Acquisition System (ATLAS) buoys, while ocean surface currents were measured by four subsurface Acoustic Doppler Current Profiler (ADCP) moorings. Three ATLAS buoys at (1.5°N, 80.5°E), (0°, 80.5°E), and (1.5°S, 80.5°E) and one ADCP mooring

at (0°, 80.7°E) were deployed before MISMO using the Indian oceanographic R/V *Sagar Kanya* (chief scientist: V. S. N. Murty, NIO) as part of a collaboration between the U.S. Pacific Marine Environmental Laboratory (PMEL)/National Oceanic and Atmospheric Administration (NOAA) and National Institute of Oceanography (NIO), India (McPhaden et al. 2006). Observations from these moorings continued after the MISMO campaign because they are part of the sustained Indian Ocean observing system (Meyers and Boscolo 2006).

Maldives observational sites. To investigate the atmospheric synoptic features over the central equatorial Indian Ocean, observational sites on three islands were established to construct an array with the

TABLE 1. List of measurement systems on board the R/V *Mirai* and principal investigators.

	Instruments	Sampling	Principal investigators
1	5.3-GHz Doppler radar	Continuously in leg 1, 2 1 volume scan = 10 min	K. Yoneyama (JAMSTEC)
2	Radiosonde	277 times in leg 1 (8/day) 52 times in leg 2 (4/day)	
3	Ceilometer	Continuously in leg 1, 2	
4	Total Sky Imager	Every 5 min in daytime in leg 1	
5	Surface meteorological station with portable radiation package	Continuously in leg 1, 2	
6	Sea surface water monitor	Continuously in leg 1, 2	
7	Shipboard ADCP	Continuously in leg 1, 2	
8	Sea-snake floating thermistor	Continuously in leg 1	
9	ISAR	Continuously in leg 1, 2	P. J. Minnett (University of Miami), R. M. Reynolds (RMR Co.)
10	Near surface towed thermometer	Continuously in leg 1	H. Kawamura (Tohoku University)
11	Turbulent flux measurement system	Continuously in leg 1, 2	O. Tsukamoto (Okayama University)
12	CO ₂ flux measurement system	Continuously in leg 1	
13	Wind profiler	Continuously in leg 1	H. Hashiguchi (Kyoto University)
14	Mie-scattering lidar	Continuously in leg 1, 2	N. Sugimoto (National Institute of Environmental Studies)
15	95-GHz cloud radar	Continuously in leg 1, 2	H. Okamoto (Tohoku University)
16	Sky radiometer	Continuously in leg 1, 2	K. Aoki (University of Toyama)
17	Videosonde	13 times in leg 1	K. Suzuki (Yamaguchi University)
18	Ozone and water vapor sonde	15 times in leg 1	M. Fujiwara (Hokkaido University)
19	Rain and water vapor sampler	Continuously in leg 1, 2	N. Kurita (JAMSTEC)
20	GPS receiver	Continuously in leg 1, 2	M. Fujita (JAMSTEC)
21	CTD with water sampling	207 times in leg 1	K. Yoneyama (JAMSTEC), S. P. Kumar (NIO, India)
22	Compact CTD with fluorometer	205 times in leg 1	N. Nakatani (Osaka Prefecture University)
23	Argo float	12 times along 80°E	N. Sato, N. Shikama (JAMSTEC)

TABLE 2. Summary of moored buoy array.

Buoy type	Equipped sensors ^a	Location	Moored period	Principal investigators
m-TRITON	AT, RH, W, R, SW, ST, C, P, CM, TH ^b	0°, 79°E	25 Oct–24 Nov	Y. Masumoto (JAMSTEC/U. Tokyo)
		0°, 82°E	27 Oct–22 Nov	
ATLAS ^c	AT, RH, W, R, SW, (LW, BP) ^d ST, C, P, CM	1.5°N, 80.5°E	3 Sep–continued	M. J. McPhaden (PMEL)
		0°, 80.5°E	5 Sep–continued	
		1.5°S, 80.5°E	6 Sep–continued	
Subsurface ADCP	ADCP ^{c,e}	1.5°N, 80.5°E	24 Oct–30 Nov ^f	Y. Masumoto
		0°, 79°E	25 Oct–24 Nov	
		1.5°S, 80.5°E	26 Oct–1 Dec	
		0°, 82°E	27 Oct–22 Nov	
		0°, 80.7°E	22 Sep–continued	M. J. McPhaden

^a Symbols for equipped sensors are air temperature (AT), relative humidity (RH), anemometer (W), rain gauge (R), and shortwave radiation (SW), for surface meteorological measurements, and sea temperature (ST), salinity (C), pressure (P), and current meter (CM) for underwater measurements. Underwater sensors measure down to 500-m depth.

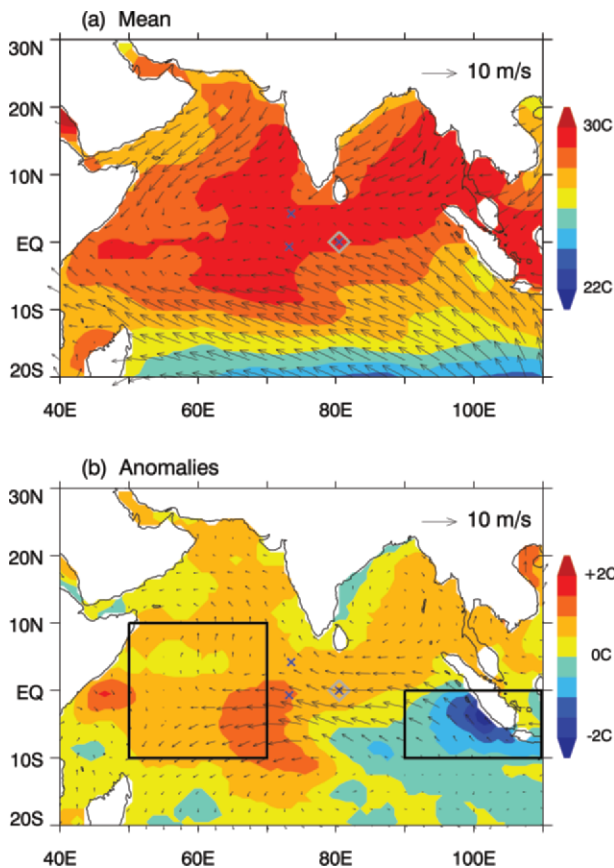
^b Thermistors (TH) were optionally attached to the hull of standard m-TRITON buoy at 0-, 25-, 50-, 100-, and 150-cm depth (Principal investigator: H. Kawamura, Tohoku University).

^c Three ATLAS buoys and one ADCP mooring at 0°, 80.7°E were deployed by the R/V *Sagar Kanya*, India.

^d Longwave radiation (LW) and barometric pressure (BP) sensors are equipped only on ATLAS buoy at 0°, 80.5°E.

^e ADCP head positioned at about 300-m depth (250 m for 0°, 80.7°E).

^f No data are available.



R/V *Mirai*. These islands were Gan (0.7°S, 73.2°E), Kadhdhoo (1.9°N, 73.5°E), and Hulhule (4.2°N, 73.5°E). Observations at the Maldives are summarized in Table 3. Radiosonde soundings at Gan Island contain extended observations for the period from 22 September through 26 December. However, due to technical difficulties, radiosonde observations were not conducted from 19 October through 30 October.

EARLY RESULTS FROM MISMO. *General conditions during the MISMO campaign.* Before showing the observational results, large-scale atmospheric and oceanic conditions during the MISMO observation period are briefly reviewed. We note that MISMO took place during a positive phase of the IOD and during a weak-to-moderate strength El Niño, both of which

FIG. 3. (a) Monthly mean SST and wind for November 2006. (b) Anomalies of the monthly mean values from the climatology (1971–2000 mean for sea surface temperature, and 2000–06 mean for sea surface wind). Crosses indicate the atmospheric sounding sites (*Mirai*, Gan, and Hulhule) and gray diamond indicates the moored buoy array. Two boxes in (b) indicate the area that is used to calculate Dipole Mode Index (DMI; cf. Fig. 4).

tended to suppress convection in the warm pool regions of the eastern Indian Ocean and western Pacific (McPhaden 2008). Figure 3a shows the monthly mean SST in the Indian Ocean for November 2006. We utilized weekly SST data from optimum interpolation SST analysis of NOAA (Reynolds et al. 2002). The highest SST is located in the central Indian Ocean, while low SST exists in the southeastern Indian Ocean off Sumatra Island. This feature is more evident by showing anomalies from climatology (Fig. 3b), which highlight the occurrence of a positive Indian Ocean Dipole event in 2006 (Vinayachandran et al. 2007). Indeed, time series of the dipole mode index shows that the MISO IOP corresponded to the mature and decaying phase of the 2006 IOD event (Fig. 4). In correspondence with this condition, anomalies of monthly mean Quick Scatterometer (QuikSCAT) sea surface winds (Fig. 3b) show the anomalous westward flow along the equator. When we look near the equator for monthly mean winds in Fig. 3a, easterlies prevailed in the eastern Indian Ocean, while westerlies dominated in the western equatorial Indian Ocean. As a result, low-level convergence existed around the Maldives Islands, suggesting favorable conditions for the development of convection over the central equatorial Indian Ocean. In addition, SSTs in the observational area were situated in the most favorable SST range (28°–30°C) for deep convection as previously reported (e.g., Zhang 1993).

Figure 5 depicts the time–longitude cross section of the outgoing longwave radiation (OLR) along the

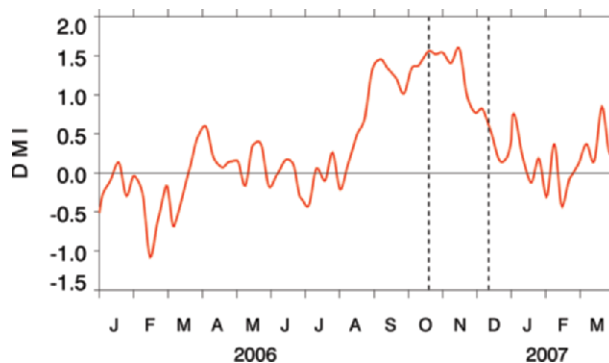


FIG. 4. Time series of DMI that is defined as anomalous SST gradient between the western tropical Indian Ocean (10°S–10°N, 50°–70°E) and the southeastern Indian Ocean (10°S–0°, 90°–110°E), after Saji et al. (1999). Dashed lines indicate the IOP.

equator averaged between 7.5°S and 7.5°N (shading). In addition, by following the work of Wheeler and Weickmann (2001), wavenumber–frequency-filtered OLR is shown by contours indicating the signals of MJOs, Kelvin waves*, and equatorial Rossby waves*. In this study, signal of the MJO convection was defined as the variability in eastward wavenumbers 1–6 and in the 30–70-day period. Several episodes of intraseasonal convective activity can be found over the MISO observation area around 80°E during this period. Although its strength is weak compared to the mid-September and late-December cases and the signal dissipated before just arriving over the maritime continent region (110°E), large-scale deep

TABLE 3. List of measurement systems and principal investigators at the Maldives sites.

Island	Location	Instruments	Observation period	Principal investigators
Hulhule	4.2°N, 73.5°E	Radiosonde	25 Oct–25 Nov (2/day)	M. Katsumata (JAMSTEC)
		Surface meteorology	22 Sep–10 Dec	
		GPS receiver	22 Sep–10 Dec	
Kadhdhoo	1.9°N, 73.5°E	Surface meteorology	22 Sep–10 Dec	
		GPS receiver	22 Sep–27 Nov	
Gan	0.7°S, 73.2°E	Radiosonde	22 Sep–18 Oct (2/day) 31 Oct–12 Nov (2/day) 13 Nov–30 Nov (4/day) 1 Dec–26 Dec (2/day)	
		Surface meteorology	22 Sep–10 Dec	
		GPS receiver	22 Sep–10 Dec	
		Ceilometer	22 Sep–10 Dec	
		9.4-GHz Doppler radar	17 Oct–30 Nov	
		Disdrometer	22 Sep–10 Dec	
		Sodar	20 Oct–10 Dec	
Skyview camera	20 Oct–25 Nov	M. Katsumata, Y. Fujiyoshi (Hokkaido University)		

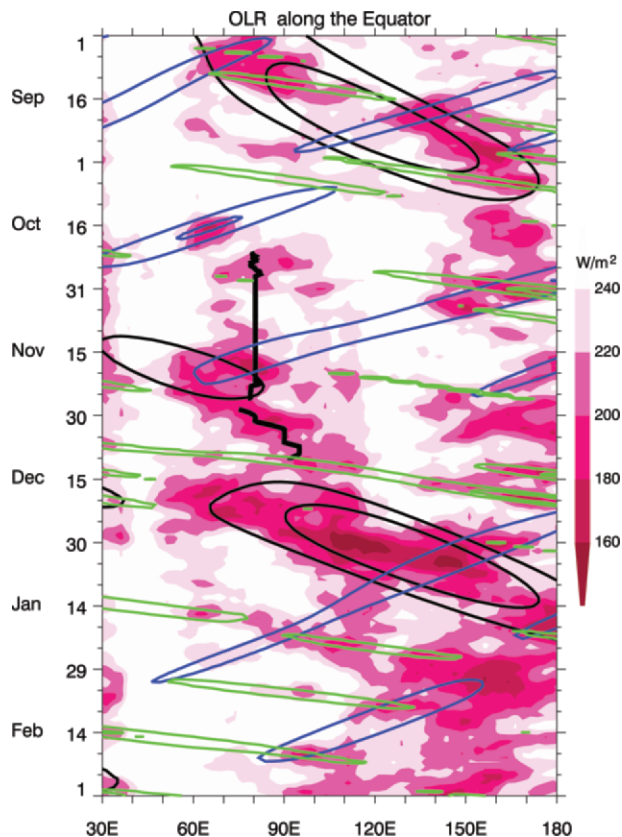


FIG. 5. Time-longitude cross section of OLR along the equator averaged over 7.5°S–7.5°N (shading). Contours are the wavenumber-frequency-filtered OLR anomalies indicating the signals identified as MJO (black), Kelvin wave (green), and equatorial Rossby wave (blue) based on Wheeler and Weickmann (2001). Contours indicate the negative anomalies and contour interval is 7.5 $W\ m^{-2}$. The position of the R/V *Mirai* is superimposed as black thick line.

cloud systems developed over the MISO area in late November and moved eastward. The filtered OLR identifies this signal as the MJO. However, there might be a controversy whether this cloud system is the MJO convection or not due to its weakness. In this paper, we therefore refer to this as the “onset of deep large-scale cloud systems on intraseasonal time scales.” Because the R/V *Mirai* cruised eastward along the equator during leg 2 in early December, the *Mirai* could trace and observe the inner structure of these eastward-moving cloud systems. In general, it can be said that MISO IOP was situated in the phase from convectively inactive to active condition and deep convection was initiated over the observational area.

Convective activity and relevant variability. In this section, the results from in situ observations will be

presented. Figure 6a shows the time series of radar echo area coverage whose reflectivity exceeds 15 dBZ at 3-km height with classification into convective/stratiform echo types following the work of Steiner et al. (1995). To compare with moisture variations, the time–height cross section of relative humidity (RH) is also depicted in Fig. 6b. After the moderately convectively active period in late October, there is a considerably suppressed period from 31 October through 4 November with no significant radar echo. During this period, very dry conditions appear above 500-hPa level and 800–600-hPa layer. The existence of a relatively high RH layer around the 500-hPa level may relate to the existence of the 0°C stable layer (Johnson et al. 1999; Ysunaga et al. 2006). After that, convective activity became moderately active and radar echo area increased. Mean echo area averaged during 6–15 November occupied about 12% of total radar observation coverage, and the high RH (over 60%) sometimes reaches above the 300-hPa level. After 16 November, the echo area greatly increased and mean echo area averaged during 16–25 November exceeded 20%. Accordingly, high RH can be found in the entire troposphere after 16 November. As for the convective and stratiform echo area ratio, while stratiform area fraction occupies 68% during 6–15 November, it increases to 74% during 16–25 November, which is comparable to the mean value over oceans measured by the Tropical Rainfall Measuring Mission (TRMM) precipitation radar (Schumacher and Houze 2003). Finally, mean stratiform echo area ratio reaches 80% during 30 November–4 December, and mean total echo area occupies over 25%. This feature of increasing stratiform echo area from inactive to active phase of intraseasonal variability is consistent with the variation of latent heating structure associated with the MJO (Lin et al. 2004).

To examine the relationship between the local conditions and convective activity, cloud height distribution that may vary in correspondence with the MJO phase was compared with the time variation of SST. Following the work of Johnson et al. (1999), we counted the daily averaged number of radar echo cells within a 160-km radius from the R/V *Mirai* in three different echo-top ranges (shallow cloud, ≤ 4 km; congestus cloud, 5–9 km; and deep cloud, ≥ 10 km). The results are shown in Fig. 7 with the time series of SST. Daily mean SST increased from a minimum value (28.3°C) on 28 October to the highest value (29.4°C) on 9 November. The diurnal cycle of SST is particularly dominant during 30 October–15 November, and skin SST measured by Infrared SST Autonomous

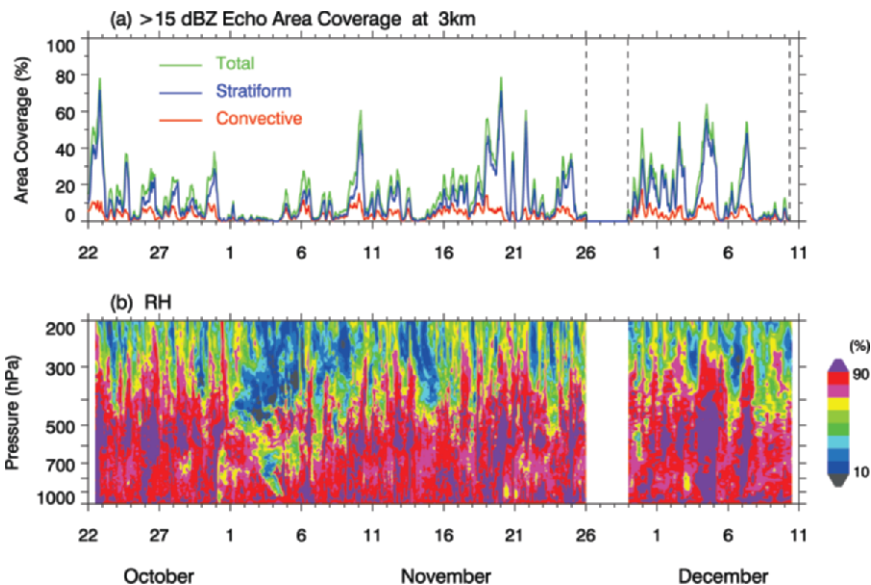


FIG. 6. (a) Time series of radar echo area coverage whose reflectivity exceeds 15 dBZ for convective (red) and stratiform (blue) types at 3-km height. Green line indicates convective plus stratiform types. Total radar observation coverage is 80,000 km². (b) Time–height cross section of relative humidity.

Radiometer (ISAR; Donlon et al. 2008) sometimes exceeded intake SST by 2°C. Such a large difference was often observed over the tropical western Pacific Ocean during the convectively suppressed period (Weller and Andersen 1996). Although a clear diurnal cycle of SST was found during 1–4 November, there were few congestus clouds. Then, the number of congestus clouds started to increase from 5 November and reached maximum during 9–12 November. The number of congestus clouds has two peaks on 9 and 15 November. Both peaks appear after a clear SST diurnal cycle continued 3–5 days. This result suggests the relationship between the diurnal cycle of SST and development of congestus clouds as previously reported (Johnson et al. 1999). The number of deep clouds also increased corresponding to the increased number of congestus clouds on 9 and 16 November.

Figure 8 shows the time–height cross section of zonal wind components

this drastic change of wind pattern in mid-November, it is possible to speculate that the equatorial Rossby wave might play a role for the onset of deep convection on intraseasonal time scales. Recently, Masunaga et al. (2006) used TRMM data to highlight cases when the onset or amplification of convection in the MJO might be induced by the interaction of the Kelvin wave with the equatorial Rossby wave.

at the R/V *Mirai* site. One notable feature is that westerlies, which prevailed at heights of 180–100 hPa in the first half of November, abruptly changed their direction to easterlies in one day (16 November). This feature is found at two other Maldives sites and even in global reanalysis datasets (not shown). By comparing the reanalysis wind field with the wavenumber frequency-filtered OLR (blue contour in Fig. 5), it was suggested that this easterly appeared in association with the westward-propagating equatorial Rossby wave. Since the large-scale cloud systems developed after

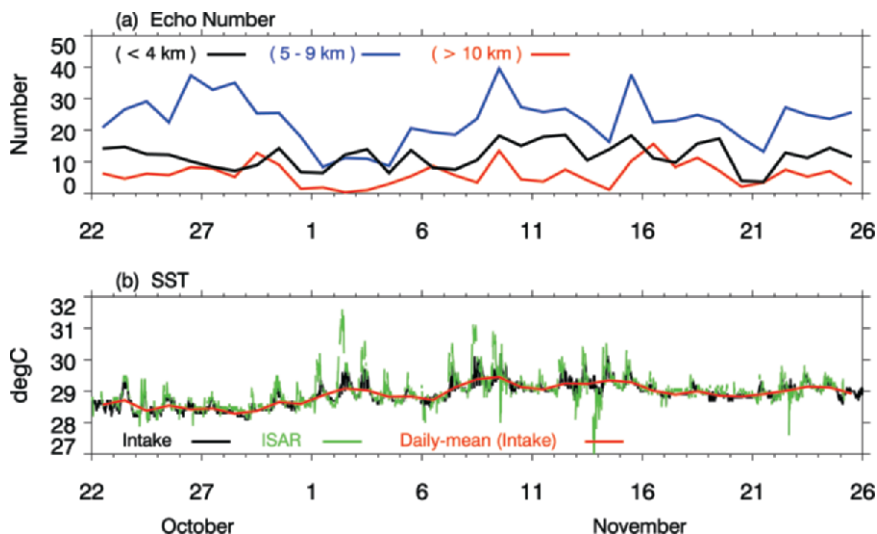


FIG. 7. Time series of (a) daily averaged echo number for the cases whose echo height is lower than 4 km (black), between 5 and 9 km (blue), and higher than 10 km (red), and (b) SST. SSTs were measured by intake sensor (roughly 5-m depth from the sea surface, black line) and ISAR system (skin surface, green line). Red line indicates daily mean value of intake SST.

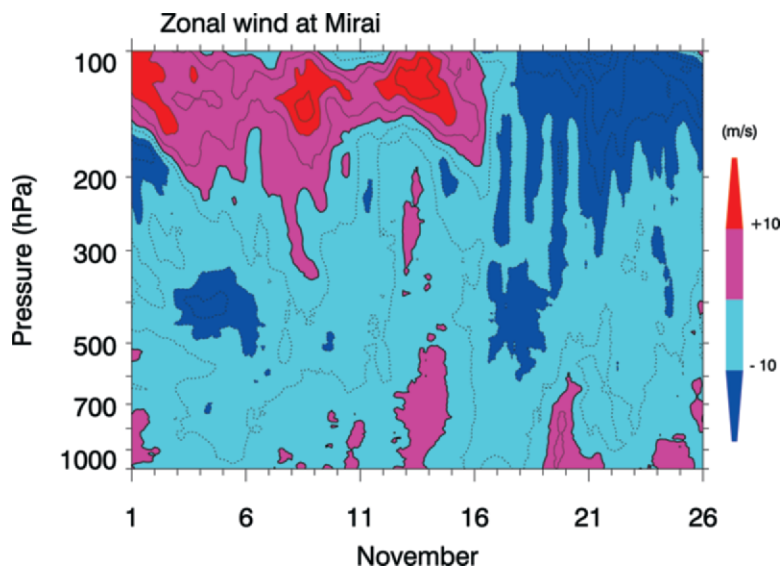


FIG. 8. Time–height cross section of zonal wind component at *Mirai*. Contour interval is 5 m s^{-1} and dashed lines indicate the negative values (easterlies).

The relationship between the equatorial Rossby wave and the development of large-scale cloud system in late November should be further studied using MISMO sounding data and satellite data.

Before the onset of large-scale cloud system, other important features are obtained. Figure 9 shows the time–height cross section of mass divergence calculated from three sounding sites. It illustrates low-level convergence throughout this period, with the strongest convergence during 16–17 November. In particular, Fig. 9 also demonstrates the gradual deepening of the strongest divergence layer from early November to late November as indicated by a dashed line. Although the strength of divergence layer in the mid- to upper troposphere is sometimes weakened (on 7–8 and 14 November), the upward shift in the layer of the peak divergence is obvious. The low-level convergence and the divergence around 150 hPa are significantly reinforced after 16 November until 25 November. By comparing Fig. 9 with Fig. 6a, we notice an interesting feature, namely, after the break of mid- to upper-tropospheric divergence layer on 7–8 and 14 November, low-level convergence (arrows in Fig. 9) and initiation of convective rain (Fig. 6a) occurred on 9 and

15 November with low-level convergence slightly leading. The latter dates also correspond to the peak in the number of congestus clouds shown in Fig. 7a. This relationship suggests that moistening of the midtroposphere by congestus clouds leads deep convection and plays a key role for preconditioning of the development of deep large-scale cloud systems shown in Fig. 5. In addition, they appeared with intervals of 5–7 days, suggesting the relationship to periodical disturbances. These features should be further studied as a next step.

Ocean variability. Although a westerly wind burst* was not observed during the MISMO IOP, oceanic observations captured various aspects of ocean surface variations. Figure 10a shows time series for surface zonal wind and precipitation, while Figs. 10b–d show time–depth cross sections of sea temperature and salinity from CTD casts and zonal currents measured by shipboard ADCP. Although the climatological surface current is eastward during this season, a westward current is found near the surface (Fig. 10d). This westward current was caused by the surface easterlies (Fig. 10a), which are related to the

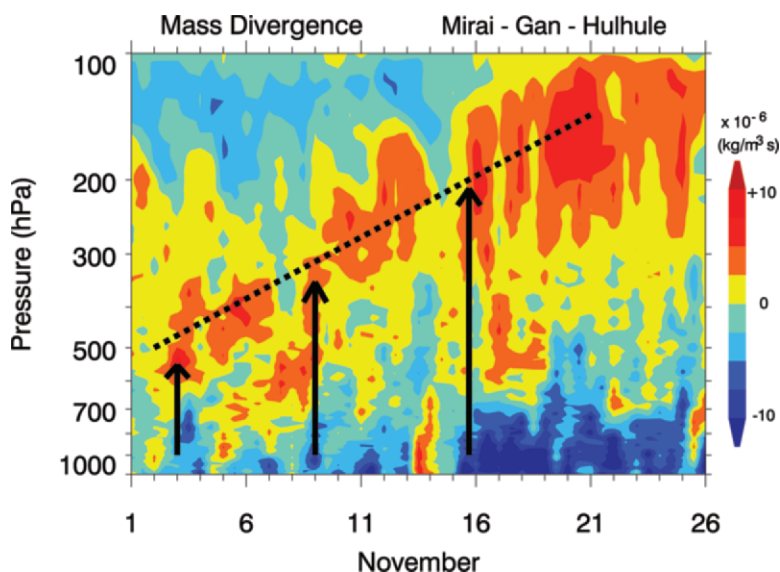


FIG. 9. Time–height cross section of mass divergence calculated over the atmospheric sounding three sites. A uniform correction for the divergence was applied to obtain the vertical velocity zero at the surface and 100-hPa level. See the text for explanation on dashed line and vertical arrows.

development of the IOD event (Horii et al. 2008). One interesting feature is that while sea temperature near the surface warmed with time (e.g., 29°C isotherm depth deepened), temperature below 150-m depth decreased (e.g., the depth of the 15°C isotherm shifted upward), resulting in a sharpened thermocline during the latter half of the observation period. This change in temperature field occurs largely during 5–10 November when the surface easterlies and accompanying ocean surface westward current became weak.

For salinity (Fig. 10c), low values (less than 34.0 psu) were found near the surface (surface–30 m) during 30 October–2 November when heavy precipitation was not observed. In addition, a subsurface maximum (greater than 35.4 psu), which decreased with time after 6 November, was found at 50–100-m depth. Since the zonal current distribution (Fig. 10d) shows the relatively strong westward (eastward) current in the surface (subsurface) layer before 6 November, zonal advection might explain these salinity variations. After mid-November, much precipitation was observed and low salinity again appeared at the surface.

These results illustrate that both temperature and salinity fields changed in structure particularly in the surface and subsurface layer during MISMO and that these variations are closely related to the behavior of the surface wind and ocean current fields. The zonal current structure is unusual compared to climatology due to the IOD event (cf. Fig. 3b), but the relationship of these variations to intraseasonal variability is unclear. Previous studies using satellite data, reanalysis products, and numerical models have suggested several possibilities. For example, Rao and Yamagata (2004) showed that intraseasonal disturbances might influence termination of the IOD, while Han et al. (2006) demonstrated that intraseasonal disturbances might have an impact on the onset of IOD. On the other hand, Shinoda and Han (2005) pointed out that IOD events reduced convective activity over

the southeast Indian Ocean. We are now analyzing MISMO data combined with longer-term data obtained by the moored buoys to address these issues, results of which will be presented in a later paper.

SUMMARY AND CONCLUDING REMARKS.

The field experiment MISMO was conducted in the central equatorial Indian Ocean during October to December 2006 with the key platforms of the R/V *Mirai*, a moored buoy array, and land-based sites in the Maldives Islands. The intensive observation period corresponded to the mature and decaying phases of an Indian Ocean Dipole event. While convective activity

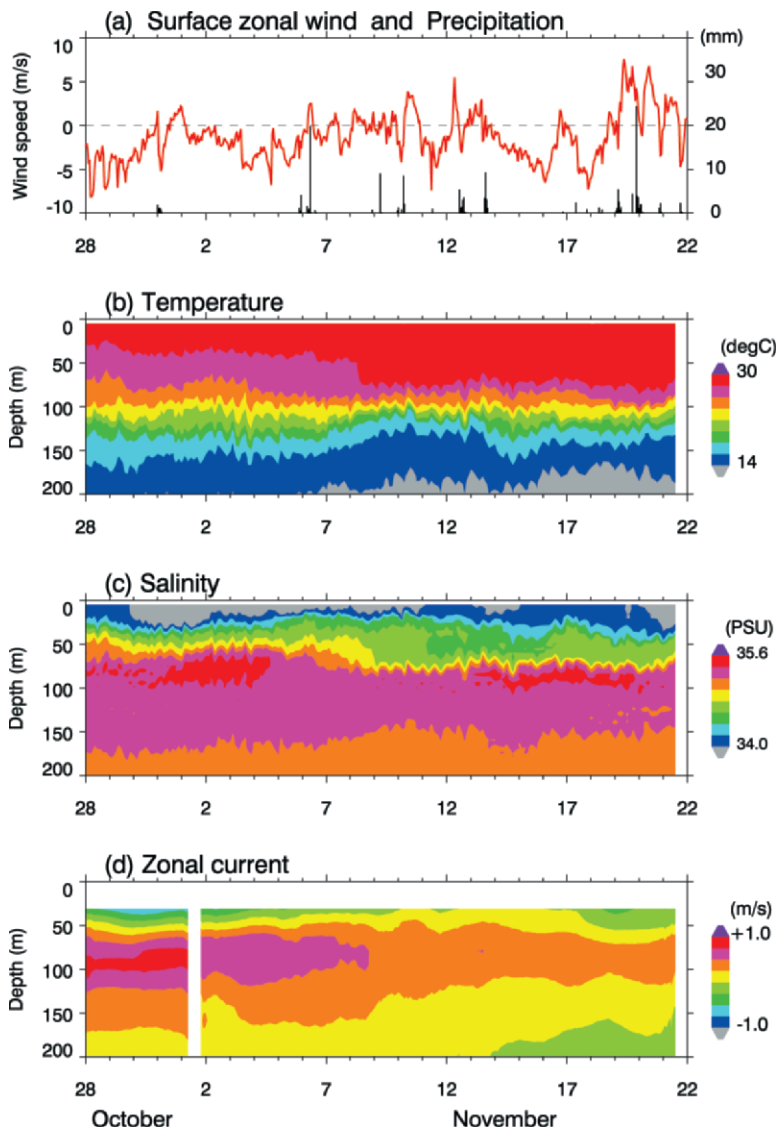


FIG. 10. (a) Time series of surface zonal wind (red) and hourly precipitation (black). Time–depth cross sections of (b) sea temperature, (c) salinity, and (d) zonal current component from *Mirai* shipboard measurements at 0°, 80.5°E. For zonal current data, a 25-h running mean is applied to reduce the error due to ship’s acceleration.

was suppressed from late October to early November, convection started to develop in mid-November, and finally much deep convection developed in the central Indian Ocean in late November. After that, eastward movement of large-scale cloud systems was observed in early December. Mainly based on the satellite data analysis, we can say that the MISMO field experiment took place during the inactive to active phase of intraseasonal convective activity.

In this article, only a few preliminary results that are mainly related to the theme of atmospheric variations are presented, with brief mention of other results related to air-sea interaction and ocean structure. Nonetheless, several interesting features were observed. Gradual deepening of the convective area was found in the divergence field (Fig. 9) before the onset of deep large-scale cloud systems in late November. It seems that several mesoscale cloud systems effectively contributed to this preconditioning as suggested from Figs. 6a and 7a. In addition, the relationship between the onset of deep large-scale cloud systems on intraseasonal time scales and equatorial waves was also suggested. The timing of the appearance of large-scale cloud systems coincided with the abrupt change of the upper-tropospheric zonal wind from westerly to easterly, and this easterly was suggested to relate to equatorial Rossby waves.

From these preliminary analyses, several important questions have been raised:

- 1) Although gradual moistening in the middle and upper troposphere was observed and it might act as a preconditioning for deep convection, which developed in late November, it seems that several mesoscale convective systems (appearing with 5- to 7-day periods) might play a key role for this moistening. If so, how did such mesoscale systems develop and what was their exact role during the preconditioning period? What is the relationship between the mesoscale and the large-scale convection?
- 2) Did the equatorial Rossby wave excite the deep large-scale convection in late November? If yes, how did they interact?
- 3) Although large-scale intraseasonal convective systems developed over the central Indian Ocean and moved eastward during the MISMO IOP, they dissipated just before arriving at the maritime continent region. Instead, after the MISMO IOP, another large-scale system, which developed in late December and was clearly identified as an MJO from the filtered OLR data, reached to the tropical western Pacific Ocean. McPhaden (2008)

suggested that warming of the eastern Indian Ocean in the wake of the 2006 event (cf. Fig. 4) preconditioned the onset of the December MJO convection. The relationship between the MJO and IOD requires further studies to verify these speculations and, for example, whether the IOD prevented convection in November 2006 from developing into an eastward-propagating wave.

We believe we can answer these questions by using not only MISMO in situ data but also in situ data from the Indian Ocean Observing System (Meyers and Boscolo 2006), satellite data including CloudSat and *Aqua* (Stephens et al. 2002), reanalysis products, and a cloud-resolving numerical model (Satoh et al. 2008).

MISMO was a challenging experiment intended to make a contribution to our understanding of the MJO from in situ observations. Although the temporal and spatial coverage of our data is limited, the authors believe that these data are valuable especially for studying detailed structure of the intraseasonal variability in the Indian Ocean. In addition, these data were the first in situ data taken during a strong IOD event. We hope these data will be used by not only MISMO participants but also by other researchers. Therefore, data collected during MISMO can be obtained from the MISMO Web site (www.jamstec.go.jp/iorgc/mismo/) beginning in January 2008. Information such as daily reports from the sites, photos, and several preliminary results can also be found there.

Recently, several observational programs including a long-term sustained observing system and process-oriented field campaigns in the Indian Ocean have been initiated (e.g., Meyers and Boscolo 2006; Duvel and Vialard 2006; Yamanaka et al. 2008), and these programs recognize that intraseasonal variability is a key component for Indian Ocean climate. Progress in MISMO data analyses will contribute to these efforts and lay the groundwork for possible future intensive observational studies of the MJO in the Indian Ocean.

ACKNOWLEDGMENTS. The authors deeply appreciate the late Dr. N. Sugimoto, the former director-general of IORGC/JAMSTEC, for his guidance to conduct the MISMO project. We also thank Captain M. Akamine and his crew of the R/V *Mirai*. Thanks are extended to technical staff of Global Ocean Development Inc. and Marine Works Japan, Ltd., for their support to the observations. Principal investigators listed in Table 1 and their colleagues are also acknowledged for their collaborative

observations. Messrs. Y. Ishihara, T. Matsumoto, and M. Yamaguchi greatly contributed to the development and deployment of the m-TRITON buoy. We would like to express our sincere thanks to the members of the Department of Meteorology of the Republic of Maldives for their observational support. We are also grateful to the CLIVAR/GOOS Indian Ocean Panel, chaired by Dr. G. Meyers, who endorsed the MISMO as a key process study and encouraged us. The moored buoy array is one of the products of this panel activity. Global OLR, NCEP–NCAR reanalysis, and optimum interpolated SST data were provided by NOAA (www.cdc.noaa.gov). QuikSCAT data are produced by Remote Sensing Systems

and sponsored by the NASA Ocean Vector Winds Science Team (www.remss.com/). The ISAR measurements were partly supported by U.S. National Ocean Partnership Program contributions by NASA and NOAA. Development of m-TRITON buoys is sponsored by the Ministry of Education, Culture, Sports, Science and Technology of Japan as a part of Japan Earth Observation System Promotion Program (JEPP). Observations at Maldivian Islands were partly supported by JEPP-HARIMAU (Hydrometeorological Array for ISV-Monsoon Auto-monitoring) project. Critical comments and suggestions from the editor and two anonymous reviewers led to the substantial improvement of the manuscript.

APPENDIX: GLOSSARY OF TERMS

The following are explanations of the terms used in this paper:

Equatorial Rossby wave: Equatorially trapped westward-propagating wave whose typical phase speed is $5\text{--}10\text{ m s}^{-1}$ and zonal scale is 60° (e.g., Kiladis and Wheeler 1995). Equatorial Rossby wave has a maximum zonal wind component on the equator.

IOD: A pattern of anomalously cool SST in the southeast Indian Ocean and anomalously warm SST in the western Indian Ocean. This situation is referred to as a positive IOD event. The opposite pattern is called the “negative IOD.”

Kelvin wave: Equatorially trapped eastward-propagating wave whose meridional component is zero. Typical phase speed and zonal scale for convectively coupled Kelvin waves are $15\text{--}20\text{ m s}^{-1}$ and $20^\circ\text{--}50^\circ$, respectively (e.g., Wheeler et al. 2000).

NCEP–NCAR reanalysis: Global gridded datasets consisting of numerical model and observation data produced by the National Centers for Environmental Prediction (NCEP) and the National Center for Atmospheric Research (NCAR). Since radiosonde sounding data taken at the MISMO three sites were sent to the meteorological operation centers through the Global Telecommunication System, some of them might be involved in the reanalysis datasets.

TOGA COARE: The Tropical Ocean and Global Atmosphere Coupled Ocean–Atmosphere Response Experiment (TOGA COARE). It was an international field experiment that took place from November 1992 through February 1993 to study the atmospheric and oceanic processes in the tropical western Pacific Ocean (Webster and Lukas 1992).

Westerly wind burst: Strong westerly wind in the lower troposphere along the equator. In this study, the definition proposed by Seiki and Takayabu (2007), which satisfies the condition that surface zonal wind anomaly exceeds 5 m s^{-1} with a zonal extent over 10° and lasting at least 2 days, was used.

Wyrтки jet: An intense eastward surface flow found at the equator in the Indian Ocean. It occurs twice a year in April–May and October–November for about 1 month and its typical maximum speed is 100 cm s^{-1} or more.

REFERENCES

- Bernie, D. J., S. J. Woolnough, J. M. Slingo, and E. Guilyardi, 2005: Modeling diurnal and intraseasonal variability of the ocean mixed layer. *J. Climate*, **18**, 1190–1202.
- Bladé, I., and D. L. Hartmann, 1993: Tropical intraseasonal oscillations in a simple nonlinear model. *J. Atmos. Sci.*, **50**, 2922–2939.
- Bond, N. A., and G. A. Vecchi, 2003: The influence of the Madden–Julian oscillation on precipitation in Oregon and Washington. *Wea. Forecasting*, **18**, 600–613.
- Donlon, C., I. S. Robinson, R. M. Reynolds, W. Wimmer, G. Fisher, R. Edwards, and T. J. Nightingale, 2008: An infrared sea surface temperature autonomous radiometer (ISAR) for deployment aboard volunteer observing ship (VOS). *J. Atmos. Oceanic Technol.*, **25**, 93–113.
- Duvel, J. P., and J. Vialard, 2006: The VASCO-CIRENE experiment. *Proc. 27th Conf. on Hurricanes and*

- Tropical Meteorology*, Monterey, CA, AMS. [Available online at <http://ams.confex.com/ams/pdfpapers/108726.pdf>.]
- Han, W., D. M. Lawrence, and P. J. Webster, 2001: Dynamical response of equatorial Indian Ocean to intraseasonal winds: Zonal flow. *Geophys. Res. Lett.*, **28**, 4215–4218.
- , T. Shinoda, L.-L. Fu, and J. P. McCreary, 2006: Impact of atmospheric intraseasonal oscillations on the Indian Ocean dipole during the 1990s. *J. Phys. Oceanogr.*, **36**, 670–690.
- Hendon, H. H., and B. Liebmann, 1990: A composite study of onset of the Australian summer monsoon. *J. Atmos. Sci.*, **47**, 2227–2240.
- Horii, T., H. Hase, I. Ueki, and Y. Masumoto, 2008: Oceanic precondition and evolution of the 2006 Indian Ocean dipole. *Geophys. Res. Lett.*, **35**, L03607, doi:10.1029/2007GL032464.
- Hsu, H.-H., B. J. Hoskins, and F.-F. Jin, 1990: The 1985/86 intraseasonal oscillation and the role of the extratropics. *J. Atmos. Sci.*, **47**, 823–839.
- Hu, Q., and D. A. Randall, 1994: Low-frequency oscillations in radiative-convective systems. *J. Atmos. Sci.*, **51**, 1089–1099.
- Johnson, R. H., T. M. Rickenbach, S. A. Rutledge, P. E. Ciesielski, and W. H. Schubert, 1999: Trimodal characteristics of tropical convection. *J. Climate*, **12**, 2397–2418.
- Kemball-Cook, S., and B. C. Weare, 2001: The onset of convection in the Madden–Julian oscillation. *J. Climate*, **14**, 780–793.
- Kikuchi, K., and Y. N. Takayabu, 2004: The development of organized convection associated with the MJO during TOGA COARE IOP: Trimodal characteristics. *Geophys. Res. Lett.*, **31**, L10101, doi:10.1029/2004GL019601.
- Kiladis, G. N., and M. Wheeler, 1995: Horizontal and vertical structure of observed tropospheric equatorial Rossby waves. *J. Geophys. Res.*, **100**, 22 981–22 997.
- Krishnamurti, T. N., D. K. Oosterhof, and A. V. Mehta, 1988: Air-sea interaction on the time scale of 30 to 50 days. *J. Atmos. Sci.*, **45**, 1304–1322.
- Liebmann, B., H. H. Hendon, and J. D. Glick, 1994: The relationship between tropical cyclones of the western Pacific and Indian Oceans and the Madden–Julian oscillation. *J. Meteor. Soc. Japan*, **72**, 401–412.
- Lin, J.-L., B. Mapes, M. Zhang, and M. Newman, 2004: Stratiform precipitation, vertical heating profiles, and the Madden–Julian oscillation. *J. Atmos. Sci.*, **61**, 296–309.
- , and Coauthors, 2006: Tropical intraseasonal variability in 14 IPCC AR4 climate models. Part I: Convective signals. *J. Climate*, **19**, 2665–2690.
- Lin, X., and R. H. Johnson, 1996: Kinematic and thermodynamic characteristics of the flow over the western Pacific warm pool during TOGA COARE. *J. Atmos. Sci.*, **53**, 695–715.
- Madden, R. A., and P. R. Julian, 1971: Detection of a 40–50 day oscillation in the zonal wind in the tropical Pacific. *J. Atmos. Sci.*, **28**, 702–708.
- , and —, 1972: Description of global-scale circulation cells in the Tropics with a 40–50 day period. *J. Atmos. Sci.*, **29**, 1109–1123.
- Maloney, E. D., and D. L. Hartmann, 1998: Frictional moisture convergence in a composite life cycle of the Madden–Julian oscillation. *J. Climate*, **11**, 2387–2403.
- , and —, 2001: The Madden–Julian oscillation, barotropic dynamics, and north Pacific tropical cyclone formation. Part I: Observations. *J. Atmos. Sci.*, **58**, 2545–2558.
- Masumoto, Y., H. Hase, Y. Kuroda, H. Matsuura, and K. Takeuchi, 2005: Intraseasonal variability in the upper layer currents observed in the eastern equatorial Indian Ocean. *Geophys. Res. Lett.*, **32**, L02607, doi:10.1029/2004GL021896.
- Masunaga, H., T. S. L’Ecuyer, and C. D. Kummerow, 2006: The Madden–Julian oscillation recorded in early observations from the Tropical Rainfall Measuring Mission (TRMM). *J. Atmos. Sci.*, **63**, 2777–2794.
- McPhaden, M. J., 1999: Genesis and evolution of the 1997–98 El Niño. *Science*, **283**, 950–954.
- , 2008: Evolution of the 2006–2007 El Niño: The role of intraseasonal to interannual time scale dynamics. *Adv. Geosci.*, **14**, 219–230.
- , Y. Kuroda, and V. S. N. Murty, 2006: Development of an Indian Ocean moored buoy array for climate studies. *CLIVAR Exchanges*, Vol. 11, No. 4, International CLIVAR Project Office, Southampton, United Kingdom, 3–5.
- Meyers, G., and R. Boscolo, 2006: The Indian Ocean Observing System (IndOOS). *CLIVAR Exchanges*, Vol. 11, No.4, International CLIVAR Project Office, Southampton, United Kingdom, 2–3.
- Nitta, T., and T. Motoki, 1987: Abrupt enhancement of convective activity and low-level westerly burst during the onset phase of 1986–87 El Niño. *J. Meteor. Soc. Japan*, **65**, 497–506.
- Rao, S. A., and T. Yamagata, 2004: Abrupt termination of Indian Ocean dipole events in response to intraseasonal disturbances. *Geophys. Res. Lett.*, **31**, L19306, doi:10.1029/2004FLO20842.
- Raymond, D. J., 2001: A new model of the Madden–Julian oscillation. *J. Atmos. Sci.*, **58**, 2807–2819.

- Reynolds, R. W., N. A. Rayner, T. M. Smith, D. C. Stokes, and W. Wang, 2002: An improved in situ and satellite SST analysis for climate. *J. Climate*, **15**, 1609–1625.
- Saji, N. H., B. N. Goswami, P. N. Vinayachandran, and T. Yamagata, 1999: A dipole mode in the tropical Indian Ocean. *Nature*, **401**, 360–363.
- Satoh, M., T. Matsuno, H. Tomita, H. Miura, T. Nasuno, and S. Iga, 2008: Nonhydrostatic icosahedral atmospheric model (NICAM) for global cloud resolving simulations. *J. Comput. Phys.*, **227**, 3486–3514.
- Schumacher, C., and R. A. Houze Jr., 2003: Stratiform rain in the tropics as seen by the TRMM precipitation radar. *J. Climate*, **16**, 1739–1756.
- Seiki, A., and Y. N. Takayabu, 2007: Westerly wind bursts and their relationship with intraseasonal variations and ENSO. Part I: Statistics. *Mon. Wea. Rev.*, **135**, 3325–3345.
- Seo, K.-H., and K.-Y. Kim, 2003: Propagation and initiation mechanisms of the Madden-Julian oscillation. *J. Geophys. Res.*, **108**, 4384, doi:10.1029/2002JD002876.
- Shinoda, T., and W. Han, 2005: Influence of the Indian Ocean Dipole on atmospheric subseasonal variability. *J. Climate*, **18**, 3891–3909.
- Slingo, J. M., and Coauthors, 1996: Intraseasonal oscillations in 15 atmospheric general circulation models: Result from an AMIP diagnostic subproject. *Climate Dyn.*, **12**, 325–357.
- , P. Inness, R. Neale, S. Woolnough, and G.-Y. Yang, 2003: Scale interactions on diurnal to seasonal timescales and their relevance to model systematic errors. *Ann. Geophys.*, **46**, 139–155.
- Sperber, K. R., 2003: Propagation and the vertical structure of the Madden-Julian oscillation. *Mon. Wea. Rev.*, **131**, 3018–3037.
- Steiner, M., R. A. Houze Jr., and S. E. Yuter, 1995: Climatological characterization of three-dimensional storm structure from operational radar and rain gauge data. *J. Appl. Meteor.*, **34**, 1978–2007.
- Stephens, G. L., and Coauthors, 2002: The CloudSat mission and the A-train: A new dimension of space-based observations of clouds and precipitation. *Bull. Amer. Meteor. Soc.*, **83**, 1771–1790.
- Tian, B., D. E. Waliser, E. J. Fetzer, B. H. Lambrigtsen, Y. Yung, and B. Wang, 2006: Vertical moist thermodynamic structure and spatial-temporal evolution of the MJO in AIRS observations. *J. Atmos. Sci.*, **63**, 2462–2485.
- Vinayachandran, P. N., J. Kurian, and C. P. Neema, 2007: Indian Ocean response to anomalous conditions in 2006. *Geophys. Res. Lett.*, **34**, L15602, doi:10.1029/2007GL030194.
- Waliser, D. E., R. Murtugudde, and L. E. Lucas, 2003: Indo-Pacific Ocean response to atmospheric intraseasonal variability: 1. Austral summer and the Madden-Julian Oscillation. *J. Geophys. Res.*, **108**, 3160, doi:10.1029/2002JC001620.
- Wang, B., and T. Li, 1994: Convective interaction with boundary-layer dynamics in the development of a tropical intraseasonal system. *J. Atmos. Sci.*, **51**, 1386–1400.
- Webster, P. J., and R. Lukas, 1992: TOGA COARE: The Coupled Ocean-Atmosphere Response Experiment. *Bull. Amer. Meteor. Soc.*, **72**, 1377–1416.
- Weller, R. A., and S. P. Andersen, 1996: Surface meteorology and air-sea fluxes in the western equatorial Pacific warm pool during the TOGA Coupled Ocean-Atmosphere Response Experiment. *J. Climate*, **9**, 1959–1990.
- Wheeler, M., and K. M. Weickmann, 2001: Real-time monitoring and prediction of modes of coherent synoptic to intraseasonal tropical variability. *Mon. Wea. Rev.*, **129**, 2677–2694.
- , and G. N. Kiladis, and P. J. Webster, 2000: Large-scale dynamical fields associated with convectively coupled equatorial waves. *J. Atmos. Sci.*, **57**, 613–640.
- Woolnough, S. J., F. Vitart, and M. A. Balmaseda, 2007: The role of the ocean in the Madden-Julian oscillation; Implications for MJO prediction. *Quart. J. Roy. Meteor. Soc.*, **133**, 117–128.
- Wyrtki, K., 1973: An equatorial jet in the Indian Ocean. *Science*, **181**, 262–264.
- Yamanaka, M. D., and Coauthors, 2008: HARIMAU radar-profiler network over the Indonesian maritime continent: A GEOSS early achievement for hydrological cycle and disaster prevention. *J. Dis. Res.*, **3**, 78–88.
- Yasunaga, K., and Coauthors, 2006: Melting layer cloud observed during R/V Mirai cruise MR01-K05. *J. Atmos. Sci.*, **63**, 3020–3032.
- Yasunari, T., 1979: Cloudiness fluctuations associated with the northern hemisphere summer monsoon. *J. Meteor. Soc. Japan*, **57**, 227–242.
- Yoneyama, K., Y. Masumoto, Y. Kuroda, M. Katsumata, and K. Mizuno, 2006: MISMO: Mirai Indian Ocean cruise for the Study of the MJO-convection Onset. *CLIVAR Exchanges*, Vol. 11, No. 4, International CLIVAR Project Office, Southampton, United Kingdom, 8–10.
- Zhang, C., 1993: Large-scale variability of atmospheric deep convection in relation to sea surface temperature in the tropics. *J. Climate*, **6**, 1898–1913.
- , 2005: Madden-Julian oscillation. *Rev. Geophys.*, **43**, RG2003, doi:10.1029/2004RG000158.